Electronic Supplementary Material (ESI) for Journal of Materials Chemistry A.
This journal is © The Royal Society of Chemistry 2014

Supplementary Information

Metal-free and all-organic redox flow battery with polythiophene as the electroactive species

S.H. Oh,[ab] C.-W. Lee,[a] D.H. Chun,[c] J.-D. Jeon,[a] J. Shim,[a] K.H. Shin[a] and J.H. Yang[a]*

[a] Energy Storage Laboratory, Korea Institute of Energy Research, Daejeon 305-343, Republic of Korea.
[b] Department of Chemical Engineering, Hanyang University, Seoul 133-791, Republic of Korea.
[c] Clean Fuel Laboratory, Korea Institute of Energy Research, Daejeon 305-343, Republic of Korea.
* Corresponding author: E-mail: enviroma@kier.re.kr

Experimental Details

Electrochemical synthesis and characterization of polythiophene

Before electrochemical polymerization, thiophene monomer (0.83 M) and tetraethylammonium tetrafluoroborate ($TEABF_4$; 1.0 M) in propylene carbonate (PC) were purged with nitrogen gas for 20 min. Three electrodes (glass carbon working electrode with an effective area of 0.0707 cm^2; platinum wire counter electrode; Ag/Ag^+ reference electrode made of a silver wire in a solution of 0.01 M $AgNO_3$ in acetonitrile) were immersed in the above solution. The potential applied to the working electrode was increased from 0.0 to 2.2 V at a rate of 100 mV s^{-1}. The total coulombic charge passing through the working electrode was recorded to estimate the amount of polythiophene synthesized electrochemically on the electrode. The polythiophene-coated working electrode was rinsed with a 1.0 M $TEABF_4$/PC solution to eliminate residual thiophene monomer. Cyclic voltammetry tests were performed in the refreshed 1.0 M $TEABF_4$/PC solution at room temperature.

Electrochemical characterization of chemically synthesized polythiophene

Polythiophene was purchased in particle form from Rieke Metals, Inc. A mixture of polythiophene (1.0 g), polyvinylidene difluoride (PVDF) binder (0.1 g), and *N*-methylpyrrolidone (7.4 g) was pasted onto a titanium current collector with an effective area of 1.0 cm^2. The thickness of the paste was controlled with a doctor blade. The polythiophene-covered titanium electrode was stored at 50 °C in an oven for more than 24 h to completely evaporate the *N*-methylpyrrolidone solvent. Using this working electrode, the coiled Pt-wire counter electrode, and the Ag/Ag^+ reference electrode, CV and EIS tests were performed at room temperature.

Charge/discharge experiments

To investigate the charge/discharge characteristics, two types of single cells were used. First, a non-flow cell consisting of a copper current collector, a bipolar plate with an effective area of 12 cm^2, carbon felt electrodes (XF-30A, Toyobo Co., Ltd.), a polytetrafluoroethylene (PTFE) flow frame, and an anion exchange membrane (Fumasep® FAP-PP-375, Fuma-tech GmbH) was used. The volumetric porosity, volumetric active area and sheet resistance of the carbon felt electrode were 9.13 ml g^{-1}, 0.459 m^2 g^{-1} and 490.0 ohm sq^{-1}, respectively. A solution containing polythiophene (8.4 g L^{-1}) and $TEABF_4$ (1.0 M) in PC was used as the initial positive and negative electrolytes. The polythiophene was supplied in particle form by Rieke Metals, Inc. Each anodic and cathodic felt electrode was soaked in 3 mL of the electrolyte. The cell was charged to 3.2 V and then discharged to 1.6 V at a current density of 5.0, 1.0, and 0.5 mA cm^{-2} using a Maccor Series 4000 battery testing system.

As the second type of single cell, a flow cell with an active electrode area of 7.0 cm × 5.0 cm was used. Carbon felt electrodes were eliminated because they interrupted the electrolyte flow. Instead, 2 g L^{-1} of Ketjen black EC600JD was mixed into the electrolytes as a

conductive additive (specific surface area = 1270 m^2 g^{-1}). A 40-mL volume of each electrolyte was circulated through the single cell by a peristaltic pump. The cell was charged to 3.0 V and then discharged to 1.0 V at a current density of 1.0, 0.5, and 0.2 mA cm^{-2}. The entire test was performed at room temperature.

Characterization of electrode surface

The polythiophene particles were characterized by scanning electron microscopy (SEM) and X-ray diffraction (XRD). SEM images were obtained on a Hitachi S-4800 microscope at 5.0 kV; XRD patterns were obtained using a Rigaku D/Max-2500 diffractometer equipped with a Cu radiation source (λ = 1.54 Å). The diffraction patterns were measured on a 200-μm film of cast polythiophene particles before doping and after n-doping or p-doping.

Density functional theory calculations of polythiophene

Density functional theory (DFT) calculations were performed using Vienna Ab-initio Simulation Package (VASP).[1,2] The generalized gradient approximation, parameterized by Perdew, Burke, and Ernzerhof (GGA-PBE),[3] was used to describe the exchange and correlation of electrons. We used projected-augmented-wave pseudopotentials for C, H, and S ions.[4] Plane waves with an energy cutoff of 400 eV were used for expansion of the electronic wave functions, and 2×1×2 k-points Monkhorst–Pack meshes were used for integrations over the Brillouin zone.[5] Both parameters were tested carefully by the convergence of DFT energy.

Since our purpose is to investigate the geometric response of polythiophene by extra electrons or holes (n- or p- doping, respectively), polythiophene model has been designed that eight thiophenes were linearly aligned in unit cell with the size of 20×42×20 $Å^3$ along y-axis of the cell. Monomers at each end of the polythiophene were separated from adjacent monomers in the neighboring unit cells with a distance of ~10 Å: dangling bonds of the

thiophene were saturated by hydrogen. In this way, polythiophene geometry fully responded to different charge states without unit cell constraint. For analyses, these corner thiophenes were not considered. Calculated lattice parameters of polythiophene match well with experimental data ($a_{expt.}$ = 1.71 Å, $b_{expt.}$ = 1.37 Å, and $c_{expt.}$ = 1.42 Å)[6,7], and previous theoretical works.[8-10] Here, relatively large lattice constant from the DFT calculations (< 1.8%) is common trend with GGA functionals.

Table S1. Performance and limitations of various redox flow batteries

System		Types of RFB	Redox couples	Cell voltage, V	Energy Efficiency, %	Concentration limitation of active species, M	Challenges
Aqueous RFB		All vanadium [2,4,5]	$V^{3+} + e^- \rightarrow V^{2+}$ $VO^{2+} + H_2O - e^- \rightarrow VO_2^+ + 2H^+$	1.26	83	2 M in 2 M-H_2SO_4	- Low energy density - Narrow operational temperature (10~40°C)
		Zn/Br [2,3]	$Zn^{2+} + 2e^- \rightarrow Zn$ $2Br- - 2e- \rightarrow Br_2$	1.85	80	2.25 M in 0.5 M-$ZnCl_2$	- Relatively low working current density (20 mA/cm^2) - Br_2 gas evolution
		Fe/Cr [2,4,6]	$Cr^{3+} + e^- \rightarrow Cr^{2+}$ $Fe^{2+} - e^- \rightarrow Fe^{3+}$	1.18	86	1 M in 3 M-HCl	- H2 gas evolution - High operation temperature (~ 65°C) - Sluggish reaction of Cr^{2+}/Cr^{3+}
		Polysulfide/Br_2 [2]	$S_4^{2-} + 2e^- \rightarrow 2S_2^{2-}$ $3Br^- - 2e^- \rightarrow Br_3^-$	1.36	80	1.3 M in 4 M-NaBr	- Severe crossover - Br_2 gas evolution
Organic RFB	Metal coordinated	V-aetylacetonate [23]	$V^{III}(acac)_3 + e^- \rightarrow V^{II}(acac)_3$ $V^{III}(acac)_3 - e^- \rightarrow V^{IV}(acac)_3$	2.2	~20	0.6 M in CH_3CN	- Low solubility of active species - Low cell voltage
		Cr-aetylacetonate [2,22]	$Cr^{III}(acac)_3 + e^- \rightarrow Cr^{II}(acac)_3$ $Cr^{III}(acac)_3 - e^- \rightarrow Cr^{IV}(acac)_3$	3.4	20	0.4 M in CH_3CN	- Low solubility of active species - Sluggish reduction of $[Cr(acac)_3]^+$
		Ru-aetylacetonate [25,26]	$Ru^{III}(acac)_3 + e^- \rightarrow Ru^{II}(acac)_3$ $Ru^{III}(acac)_3 - e^- \rightarrow Ru^{IV}(acac)_3$	1.75	57	NG	- Irreversible side reaction - Low state of charge
		Mn-aetylacetonate [23,24]	$Mn^{III}(acac)_3 + e^- \rightarrow Mn^{II}(acac)_3$ $Mn^{III}(acac)_3 - e^- \rightarrow Mn^{IV}(acac)_3$	1.1	21	0.6 M in CH_3CN	- Low cell voltage - Irreversible side reaction
		Ru-bipyridine [27]	$Ru^{III}(bpy)_3^{3+} + e^- \rightarrow Ru^{II}(acac)_3^{2+}$ $Ru^{III}(acac)_3^{3+} - e^- \rightarrow Ru^{IV}(acac)_3^{4+}$	2.6	NG	0.2 M in CH_3CN	- Poor chemical stability - Low solubility of active species
		Ni,Fe-bipyridine [28,29]	$Ni(bpy)_3 + 2e^- \rightarrow Ni^{II}(bpy)_3^{2+}$ $Fe^{II}(bpy)_3^{2+} - e^- \rightarrow Fe^{III}(bpy)_3^{3+}$	2.2	82	0.4 M in propylene carbonate	_Ion crossover _High polarization
	Metal free	TEMPO/ N-Methylphthalimide [20]	N-Methylphthalimide + e^- → radical anion TEMPO - e^- → radical cation	1.6	74	0.1 M in CH_3CN	_Low solubility of active species _Low cell voltage
		2,5-di-tert-butyl-1,4-bis(2-methoxy ethoxy)benzene/ 2,3,6-trimethylquinoxaline [21]	2,3,6-trimethylquinoxaline + e^- → radical cation DBBB - e^- → radical cation	1.8	37	0.4 M in propylene carbonate	_Low energy density _Low solubility of active species

NG: not given

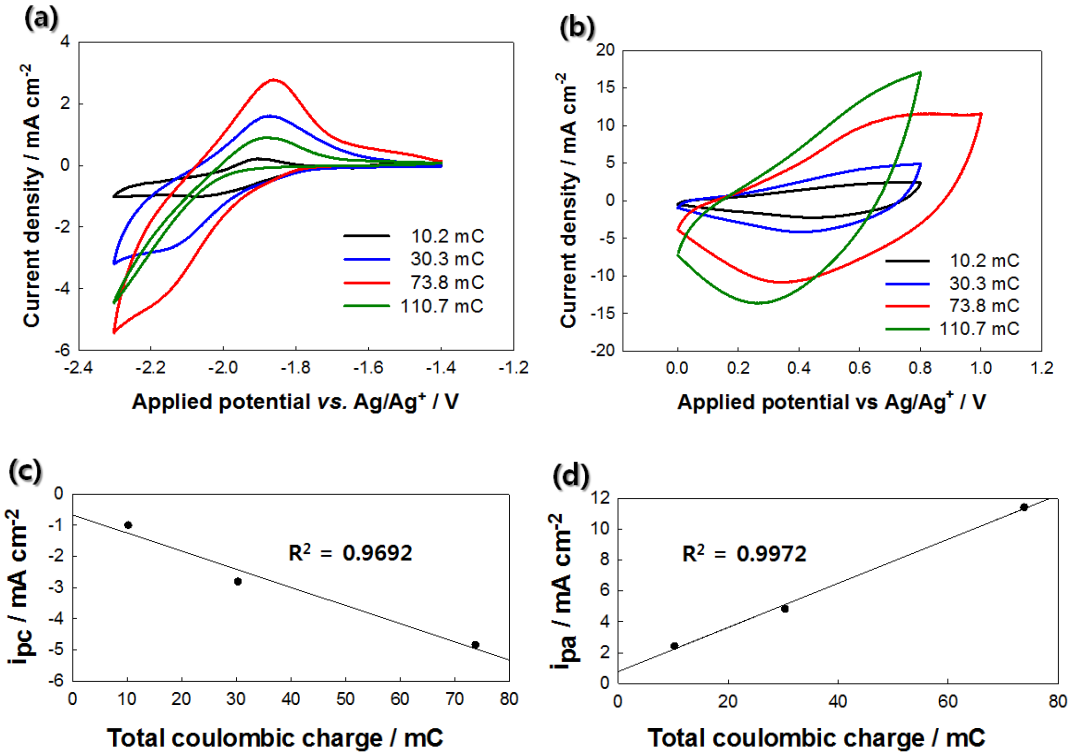

Figure S1. Cyclic voltammograms of polythiophene polymerized at different levels of deposition charge. Cyclic voltammogram for (a) n-doping and (b) p-doping. (c) Total coulombic charge dependence of cathodic peak current density in n-doping process. (d) Total coulombic charge dependence of anodic peak current density in p-doping process.

When the polythiophene layer became thicker than a certain value, the charge-transfer reaction for n-doping was sharply weakened (Fig. S1). We adjusted the thickness of polythiophene synthesized on the carbon electrode by applying different deposition charges during the electrochemical polymerization. The cathodic peak current density for n-doping increased linearly with deposition charge ranging from 10.2 to 73.8 mC. However, the overpotential was significantly increased and the current density was decreased at a charge of 110.7 mC.

Unlike the case for n-doping, the anodic peak current density for p-doping increased linearly with the deposition charge over the entire range from 10.2 to 110.7 mC

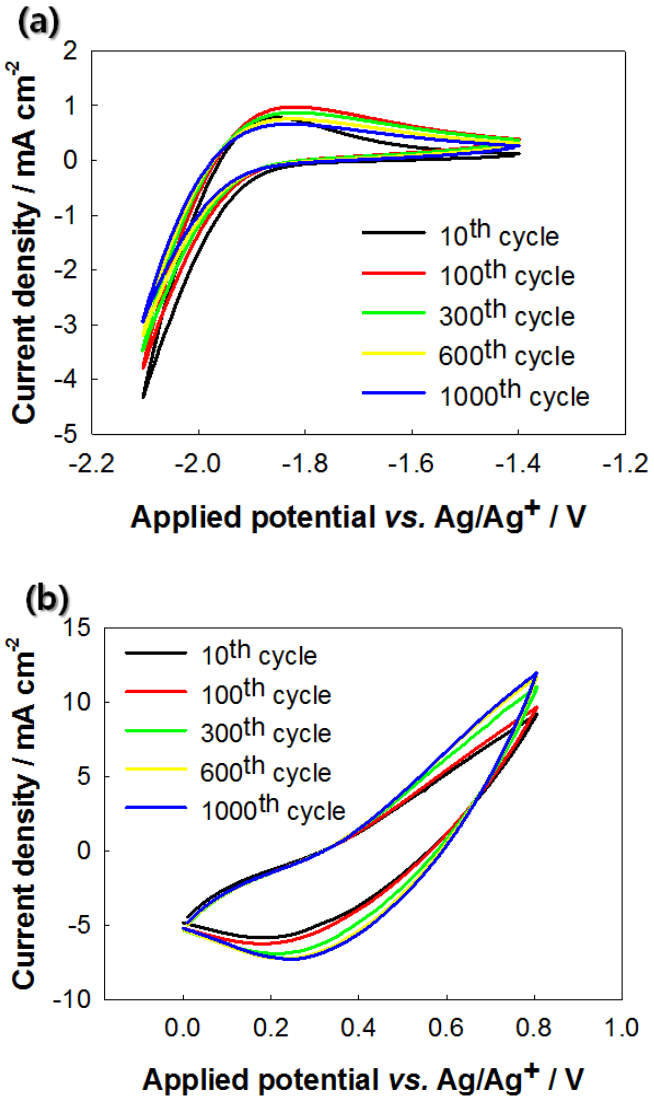

Figure S2. Cyclic voltammograms of 200-µm film of cast polythiophene particles for (a) n-doping and (b) p-doping. 1000 cycles, sweep rate: 100 mV s^{-1}, electrolyte 1 M $TEABF_4$ in propylene carbonate.

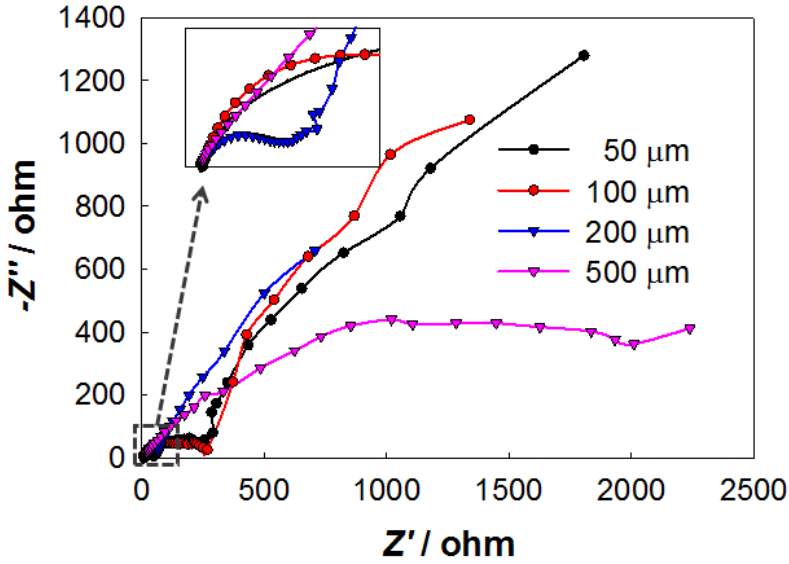

Figure S3. Impedance measurements in Nyquist form of a polythiophene microparticle layer coated on a titanium electrode. The measurements were obtained at a frequency range of 100 kHz to 1 mHz, with potential perturbations measuring 10 mV in amplitude.

According to the EIS analysis, the polythiophene layers with thicknesses of 50, 100, and 200 µm followed the Mansfeld-circuit model,[11-13] while the 500-µm layer showed more complicated behaviour

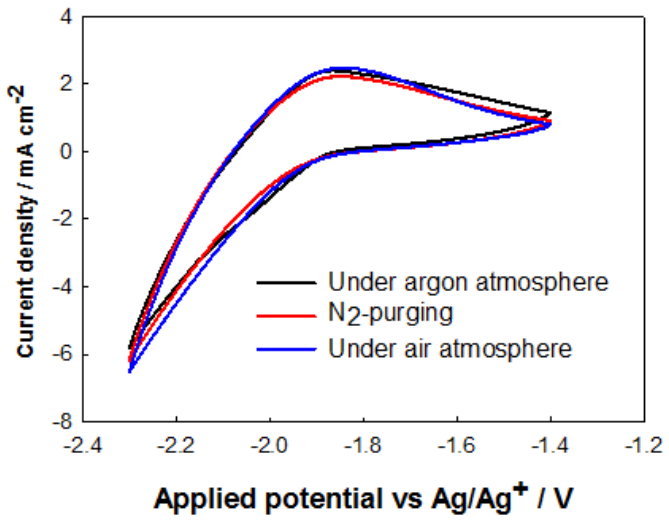

Figure S4. Cyclic voltammograms of 200-µm film of cast polythiophene particles prepared under different degrees of air exposure. 20 cycles, sweep rate: 100 mV s^{-1}, electrolyte 1 M $TEABF_4$ in propylene carbonate.

To identify the air sensitivity of the electrode reactions, we have performed three different experiments with various degree of air exposure. First, we have prepared the electrolyte and performed the cyclic voltammetry test in a glove box under argon atmosphere. Secondly, the electrolyte was prepared under air atmosphere and purged with N_2-gas for 20 minutes. And then the cyclic voltammetry was performed for the electrolyte. Finally, the electrolyte prepared under air atmosphere was tested without N_2-purging.

We observed little difference in peak current density among these three tests. Therefore, we could conclude that polythiophene was not air-sensitive.

Table S2. Theoretical bond angles of polythiophene. Numbers in parentheses (n- and p-doping) indicate angular deviations with respect to neural counterpart of corresponding angle.

	a'	b'	c'	d'	e'
Neutral	109.87	113.64	113.64	109.90	92.95
p-doping	110.75 (+0.88)	113.24 (-0.40)	113.25 (-0.39)	110.80 (+0.90)	91.97 (-0.99)
n-doping	108.88 (-0.99)	114.47 (+0.83)	114.59 (+0.95)	108.92 (-0.98)	93.14 (+0.18)

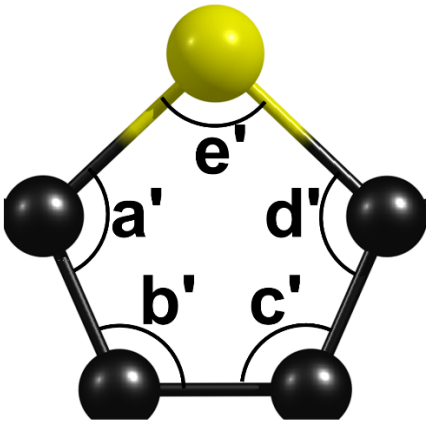

Figure S5. Schematic description of inner angle labels for polythiophene

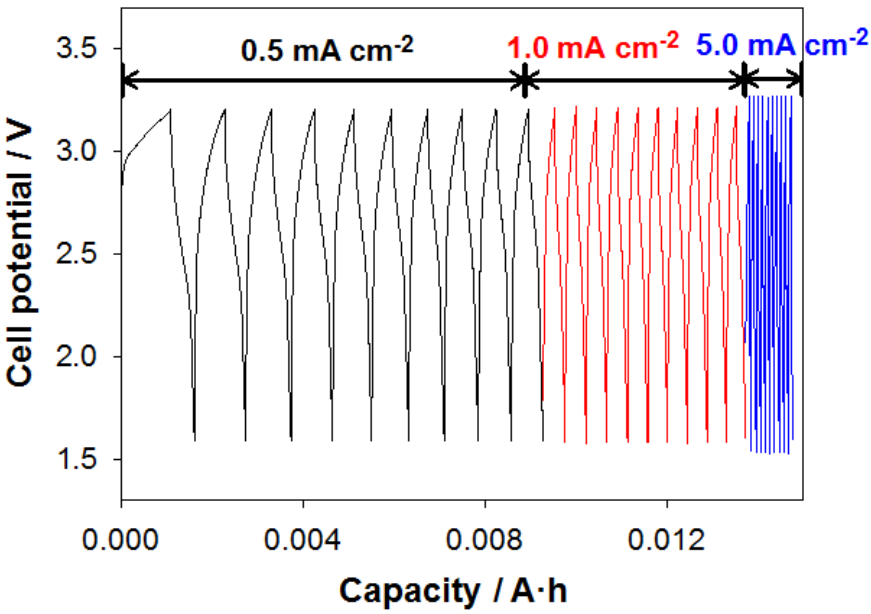

Figure S6. Charge/discharge profile of the non-flow cell at different current densities and 25 °C.

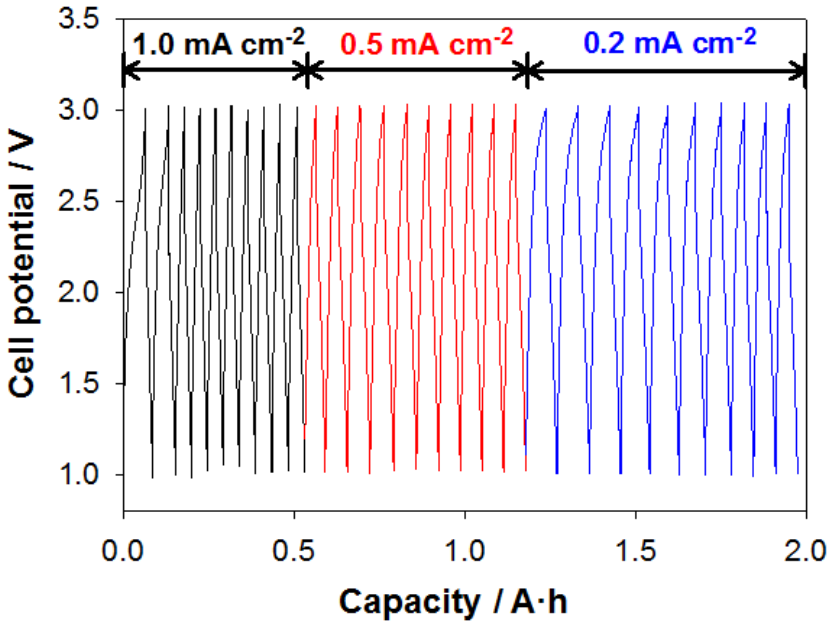

Figure S7. Charge/discharge profile of the flow cell at different current densities and 25 °C.

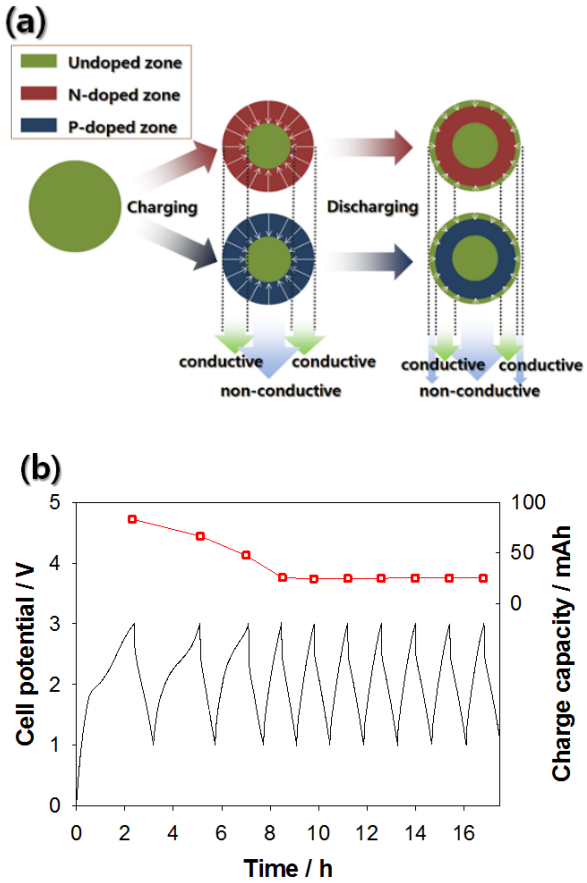

Figure S8. (a) Schematic diagram of variations in the conduction zone of a polythiophene particle during charging and discharging. (b) Charge/discharge profile and variations in charge capacity during the first few cycles at 1.0 mA cm^{-2}.

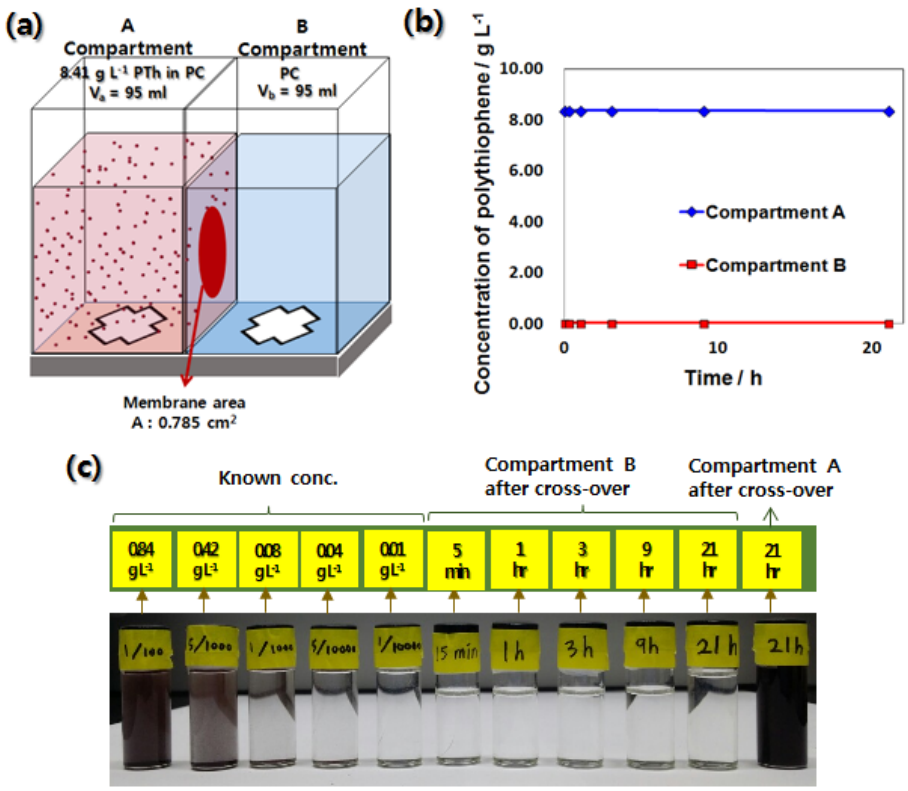

Figure S9. (a) Schematic diagram of a home-made apparatus for cross-over test. (b) Polythiophene concentration variation with time. (c) Photo images for the sampled solution during the cross-over test.

While the separator (Fumasep® FAP-PP-375, Fuma-tech GmbH) used in this study was the non-porous functional anion-exchange membrane, the polythiophene particles had a measurable size of 7.32 μm (average). Therefore, there was little cross-over of the particles through the membrane.

Polythiophene cross-over properties of the anion-exchange membrane were measured using a home-made apparatus given in Fig. S9a. Initially, compartment B (95 mL) was filled with pure propylene carbonate and then, compartment A (70mL) was filled with a solution containing polythiophene (8.41 g L^{-1}) in propylene carbonate. The membrane, diffusion area of 0785 cm^2, was sandwiched by O-ring shaped rubber on purpose of sealing and clamped between the two compartments tightly. The diffusion cell was kept stirring slowly during the experiment to avoid concentration polarization. The concentration of polythiophene diffused

from the compartment A to B across the membrane was detected with time using a ultra-violet spectrometer. The concentration variation of polythiophene with time is shown in Fig. S9b. The polythiophene concentration in compartment B remained below 0.04 g L^{-1} during 21-h test. Therefore, we could conclude that the polythiophene cross-over through the membrane was negligible.

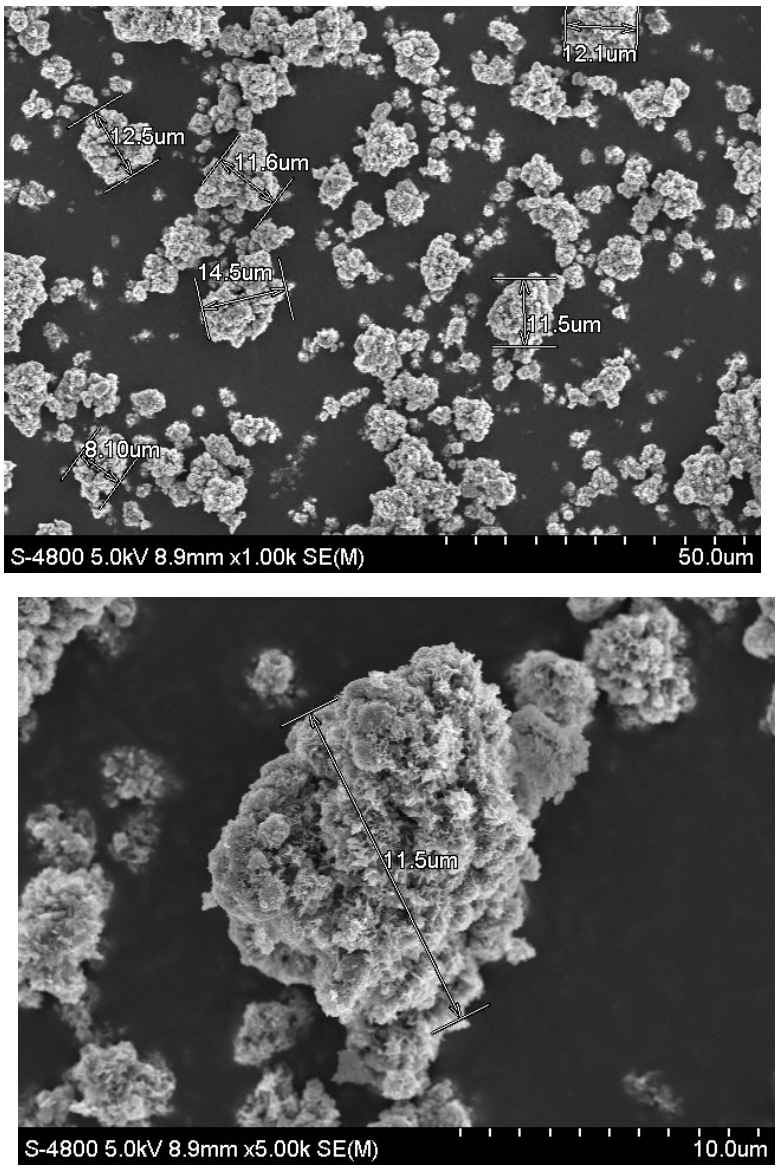

Figure S10. SEM images for polythiophene particles

References

1. G. Kresse and J. Furthmüller, *Phys. Rev. B*, 1996, **54**, 11169.

2. G. Kresse and D. Joubert, *Phys. Rev. B,* 1999*,* **59**, 1758.

3. J. P. Perdew, K, Burke and M. Ernzerhof, *Phys. Rev. Lett.*, 1996, **77**, 3865.

4. P. E. Blöchl, *Phys. Rev. B*, 1994, **50**, 17953.

5. H. J. Monkhorst and J. D. Pack, *Phys. Rev. B*, 1976, **13**, 5188.

6. J.S. Kwiatkowski, J. Leszczynski and I. Teca, *J. Mol. Struct.*, 1997, **451**, 436.

7. B. Bak, D. Christensen, L. Hansen-Nygaard, J. Rastrup-Andersen, *J. Mol. Spectrosc.*, 1961, **7**, 58.

8. G. Brocks, *J. Phys. Chem.*, 1996, **100**, 17327.

9. A. M. Asaduzzaman, K. Schmidt-D'Aloisio, Y. Dong and M. Springborg, *Phys. Chem. Chem. Phys.*, 2005, **7**, 2714.

10. S. P. Rittmeyer and A. Groß, *Beilstein J. Nanotechnol.*, 2012, **3**, 909.

11. P.L. Bonora, F. Deflorian and L. Fedrizzi, *Electrochim. Acta,* 1996, **41**, 1073.

12. F. Mansfeld, M. Kendig and S. Tsai, *Corrosion,* 1982, **38**, 478.

13. F. Mansfeld, M. Kendig and S. Tsai, *Corrosion Sci.,* 1983, **23**, 317.